数理解析研究所講究録
1121 巻 2000 年 256-269

Subgrid-scale energy transfer と渦層・渦管

東工大・工学部　堀内　潔

1 Introduction

Large-eddy simulation (LES) is a turbulence simulation method in which the large scale (grid scale) field is directly calculated, while the small scale (subgrid-scale or SGS) field is modeled. The velocity and pressure fields (f) are decomposed into grid-scale component ($\overline{f}$) and SGS component ($f' = f - \overline{f}$) using a filtering procedure:

$$\overline{f}(\mathbf{x}) = \int_{-\infty}^{\infty} f(\mathbf{x}')\overline{G}(\mathbf{x}, \mathbf{x}')d\mathbf{x}', \tag{1}$$

where $\overline{G}(\mathbf{x})$ denotes the filter function.

The effects of the SGS field on the grid-scale field is represented by the SGS stress tensor, $\tau_{ij} = \overline{u_i u_j} - \overline{u}_i \overline{u}_j$, which results from filtering the Navier-Stokes equations, where $u_i' = u_i - \overline{u}_i$. The energy transfer between the grid scale field and the SGS field occurs through the SGS production term, $P = -\tau_{ij}\partial\overline{u}_i/\partial x_j$. When P is non-negative, the grid scale energy is forwardly transferred into SGS (forward scatter), while if P is negative the SGS energy is in turn transferred backwardly into the grid scale (backward scatter). Recent direct assessment of the energy transfer carried out using DNS data for wall-bounded flows [1, 2, 3, 4] revealed that the energy exchange is not unidirectional. Although a mean direction of energy transfer is from the grid scale to the SGS, SGS energy is also transferred in the opposite direction to the grid scale.

One of advantages of LES is that it can estimate an energy cascade from the given scale down to the smaller scales locally in the physical space via the SGS production term, enabling a detection of events which provides intense energy transfer. Coherent structures are known to exist in the wall-bounded and free shear turbulent flows such as the streaks in the former and the rib vortices in the latter. The objective of the present study is to investigate a correlation of these coherent structures with the SGS energy transfer mechanism by utilizing the direct numerical simulation (DNS) flow fields (Sec. 2). A particular emphasis is placed on the backward scatter effect. In Sec. 3, the time development of the educed coherent structure is pursued in the actual LES.

2 Eduction of intense SGS energy production events

In this section, we educe the structures associated with the generation of intense SGS energy using a conditional averaging method.

2.1 Channel flow

The wall-bounded turbulence DNS data that we used were for fully developed incompressible channel flow with Re_τ (Reynolds number based on the wall-friction velocity, u_τ, and the half channel height, δ) =180. The Fourier-Chebyshev polynomial expansion method was used with 128, 129 and 128 grid points, respectively, in the x, y and z directions. [5, 6] In the following, y_+ denotes the wall coordinate $u_\tau y/\nu$, where ν is the kinematic viscosity.

The channel flow field was filtered to $32 \times 129 \times 32$ in the x, y and z directions, respectively. In the filtering procedure described in Eq. (1), the most common filters are Gaussian, top-hat and spectral cutoff filters. In the present study, we adopted the Gaussian filter because this filter has a localized support in physical space, which property is beneficial for the use of the scale-similarity model that we incorporate into actual LES. In the present work, no filter was applied in the inhomogeneous direction, but the same numerical discretization method was used in the inhomogeneous direction both in the direct numerical simulation (DNS) data generation and in the LES computations. Numbers of LES grid points were chosen so that the turbulent kinetic energy retained in the SGS components was large.

Figures 1 shows the $y-$distributions for plane-average of the individual terms in P, P_{ij} (no summation in i and j), in which τ_{ij} is estimated from the exact SGS stress obtained from the channel flow DNS data. These terms were decomposed into two-parts which contribute to forward and backward scatters. Significant backward scatter arises in the normal production term of P_{11} term at $y_+ \approx 15$. It can be seen that the magnitude of forward and backward scatter terms in P_{11} is very close each other, with the total sum of P_{11} being slightly positive, but the sum even becomes negative in the region at $y_+ \approx 12$. Subsequently, the root-mean-square (rms) value of P_{11} term showed a largest value among the P_{ij} terms, and the rms values were several times larger than the average values (figure not shown).

The shear production term, P_{12}, is dominant in the very vicinity of the wall ($y_+ < 10$). The energy transfer arising in this term is predominantly forward due to the presence of the large mean velocity gradient near the wall. [1, 4, 6] When the mean velocity gradient was subtracted from the estimate of P_{12} term, its magnitude was substantially reduced. Thus, the local variation of energy exchange between grid scale and SGS is better represented by P_{11} term rather than P_{12} or P terms. It can be considered that P_{11} term is more appropriate to use for the detection of the events associated with intense grid scale-SGS energy transfer.

Based on above observations, we educe the coherent structures by sampling the events with intense P_{11} term by applying a conditional averaging procedure. [4, 7] The velocity fields were averaged for the events that corresponded to strong forward and backward scatters in P_{11} term. Strong forward scatter event was detected by imposing the one-point conditions of the type $T(p_t) > 0.1$, where $T(p_t)$ is defined as

$$T(p_t) = \int_{p_t}^{\infty} fP(f)df \Big/ \int_{-\infty}^{\infty} |fP(f)|df. \tag{2}$$

Here, $P(f)$ denotes the probability function of P_{11}. Similarly, for the backward scatter

event, the conditions of $T(p_t) < -0.1$ was imposed, where $T(p_t)$ is

$$T(p_t) = \int_{-\infty}^{p_t} fP(f)df / \int_{-\infty}^{\infty} |fP(f)|df. \tag{3}$$

This detection was carried out for the grid points in the $x-z$ plane located at $y_+ = 12$. It was felt that when an excessive symmetry is imposed for the conditional averaging, important fine structures are eliminated by superposing the structures with opposite orientations.

In the previous analysis of the vortical structures in the channel, [8] it was reported that the histograms of θ, inclination angle to the $x-z$ plane of the projection of the vorticity vector in the $x-y$ planes, $\theta = \tan^{-1}(\overline{\omega}_2/\overline{\omega}_1)$, was concentrated around $\pm 90°$ in the $x-z$ plane located at $y_+ = 12$. Here, $\overline{\omega}_2$ denotes the GS normal vorticity $\overline{\omega}_2 (= \partial\overline{u}/\partial z - \partial\overline{w}/\partial x)$. This result indicates a significant contribution of the wall-normal vorticity for the vortex dynamics in the near wall region. In fact, the intensity of the shear production term of P_{13} shown in Fig. 1 is not negligible.

In order to eliminate the imposition of excessive symmetry, we further constrained the orientation of wall normal vorticity, i.e., the events with positive wall-normal vorticity $\overline{\omega}_2 > 0$ was chosen. Each time an event was detected, the whole grid scale velocity field was stored, centering on the event. All the realizations where the condition was satisfied were then averaged to yield the conditionally-averaged fields. [7] Detection was done for both lower and upper walls. Approximately 150 events with large positive P_{11} term value and a positive normal vorticity were detected and averaged from the 10 realizations of the DNS data separated by non-dimensional time interval $0.6tu_\tau/\delta$.

Figure 2 shows the contours of the streamwise velocity, $\overline{u}'' = \overline{u} - < \overline{u} >$, in the $x-z$ plane at $y_+ \approx 12$, associated with the detected events. $< f >$ denotes the average of f in the $x-z$ plane. Positive values are plotted by the solid lines, and the negative ones by the dashed lines. The flow is from left to right of the figure. Figures 2 (a) and (b) show the results obtained from the forward-scatter events ($T(p_t) > 0.1$) (referred to as the $P_{11}-$Forward event) and the the backward-scatter events ($T(p_t) < -0.1$) ($P_{11}-$Backward event), respectively. These contours show asymmetric streaky structures. In Fig. 2 (a), the region with negative contours (low speed streak) is placed downstream of that with positive contours (high speed streak) near the detection point located at the center of this $x-z$ plane. This result is similar to those obtained in Johansson *et al.* [10] using the VISA method and also those obtained using the λ_2 method in Jeong *et al.* [11].

To examine the accuracy of the educed flow field for an approximation of the "real" turbulence, the y-profiles of the grid-scale turbulence intensities are shown in Fig. 3, in which the intensities are compared with those obtained from the "exact" filtered-DNS data. Although these intensities decay much faster as the distance from the lower wall is increased, because the vortical structures in the upper half of the channel were smeared out, the overall intensity profiles are well represented qualitatively. It should be noted that, quantitatively, the amplitude of the intensities for the educed flow field is approximately a quarter of the filtered DNS data. This is because the significant portion of educed structure is concentrated near the detection point.

In the $P_{11}-$Forward event, a strong shear is generated in the region where a high speed streak catches up with a low speed streak. This region coincides with the detection

point, where a large negative value for the longitudinal velocity derivative $\partial\overline{u}/\partial x$ occurs. A large wall normal vorticity, $\overline{\omega}_2$, is generated in this region.

In the $P_{11}-$Backward event, a low speed streak is placed upstream of high speed streak as shown in Fig. 2 (b). A large positive value for the longitudinal velocity derivative $\partial\overline{u}/\partial x$ occurs in the region where a low speed streak resides adjucent to a high speed streak, and a large streamwise vorticity, $\overline{\omega}_1(=\partial\overline{w}/\partial y - \partial\overline{v}/\partial z)$, is generated here.

Figures 4 (a) and (b) show the scatter plots between the P_{11} term and the streamwise and the wall-normal vortices, respectively, which were taken from the region $9 \leq y_+ \leq 21$. It can be seen in Fig. 4 (a) that large $\overline{\omega}_1$ is associated with negative P_{11}, whereas large positive P_{11} generates no significant $\overline{\omega}_1$. In Fig. 4 (b), large $\overline{\omega}_2$ is correlated with large positive P_{11}. Thus, principal vortical structures educed in the present detection are the streamwise vortices generated along the $P_{11}-$Backward event and the wall-normal vortices generated along the $P_{11}-$Forward event.

This result can be explained by using the vortex stretching term in the governing equation for the grid-scale enstrophy $P_\omega = \overline{\omega}_i\overline{\omega}_j\partial\overline{u}_i/\partial x_j$. Major term for the streamwise enstrophy equation is the term $\overline{\omega}_1\overline{\omega}_1\partial\overline{u}_1/\partial x_1$. It can be readily seen that $P_{11}-$Backward event provides positive contribution to this term, i.e., enhances $\overline{\omega}_1$, whereas $P_{11}-$Forward event makes negative contribution i.e., reduces $\overline{\omega}_1$. Similarly, the term for the wall-normal enstrophy equation, $\overline{\omega}_2\overline{\omega}_2\partial\overline{u}_2/\partial x_2$ can be approximates as $-\overline{\omega}_2\overline{\omega}_2\partial\overline{u}_1/\partial x_1$ via the continuity equation. $P_{11}-$Forward event provides positive contribution to this term and enhances $\overline{\omega}_2$, whereas $P_{11}-$Backward event makes negative contribution i.e., reduces $\overline{\omega}_2$. [12]

In order to classify the educed vortical structures, we utilized the λ_2 method, where λ_2 denotes the second largest eigen value of the tensor $S_{ik}S_{kj} + \Omega_{ik}\Omega_{kj}$, $(S_{ij} = (\partial\overline{u}_i/\partial x_j + \partial\overline{u}_j/\partial x_i)/2, \Omega_{ij} = (\partial\overline{u}_i/\partial x_j - \partial\overline{u}_j/\partial x_i)/2)$. [11] Figure 5 shows the scatter plots between the P_{11} term and λ_2. $P_{11}-$Forward event is primarily correlated with positive λ_2, while $P_{11}-$Backward event is associated with negative λ_2. That is, the wall-normal vortices generated with the $P_{11}-$Forward event are classified as a vortex sheet, whereas the streamwise vortices generated with the $P_{11}-$Backward event are classified as a vortex tube.

In summary, forward cascade of the grid-scale energy is associated with the vortex sheet-like structure, which is consistent with the previous result for the homogeneous isotropic turbulence. [13] On the other hand, backward scatter is associated with the formation of vortex-tube like structure. Figure 6 shows the histogram for the longitudinal velocity derivative $\partial\overline{u}/\partial x$ in the $x-z$ plane at $y_+ = 12$, obtained from the filtered DNS data. Its distribution is asymmetric with respect to $\partial\overline{u}/\partial x = 0$, and skewed for negative values. This asymmetric and non-Gaussian distribution has been noticed, e.g., in Vincent *et al.* [14] We consider that this occurred so that the energy cascade becomes forward on average.

2.2 Energy transfer in mixing layer and homogeneous isotropic turbulence

In this section, we assess the correlation of the energy transfer and vortex-sheet/tube structure in mixing layer and decaying homogeneous isotropic turbulence.

For free shear turbulence, we have chosen incompressible mixing layer flow that de-

velops in time, and generated DNS data using the Fourier/finite difference method, with 192, 128 and 128 grid points, respectively, in the x, y and z directions. [6] The Reynolds number, Re_θ, based on the mean velocity difference between the two edges of the mixing layer, ΔU, and the initial momentum thickness, θ_0, was set equal to 200. The pseudospectral Fourier expansion method was used in the x and z directions, whereas the 2nd-order central finite difference method was used in the y direction. This mixing layer DNS data was filtered to $96 \times 128 \times 64$ grid points, respectively, in the x, y and z directions. Assessment was done at $t = 350$, [6] when streamwise rib vortices had been formed in the braid region between the rollers after the occurrence of a mixing transition, [15] and the flow was in a turbulent regime.

The incompressible homogeneous isotropic turbulence DNS data were generated using the pseudo-spectral method with 128, 128 and 128 grid points, respectively, in the x, y and z directions. The initial Taylor microscale Reynolds number was approximately 100. Assessment was done using the data when the Taylor microscale Reynolds number was approximately 45. This homogeneous flow DNS data was filtered to $32 \times 32 \times 32$ in the x, y and z directions, respectively.

Figures 7 shows the scatter plots between the P term and λ_2 obtained for the mixing layer flow. Forward scatter event is rather correlated with negative λ_2, indicating that energy cascade primarily occurs through a tube-like structure, presumably by a stretching of vortex tubes. The degree of an occurrence of the sheet-like structure with positive λ_2 is reduced compared with the result from the channel flow shown in Fig. 5, i.e., the tube-like structure is dominant in the mixing layer. Similar results were obtained both in the rib region and the braid region of the mixing layer. This result may be affected by the low Reynolds number for the DNS data used here. We are currently working on an assessment at the high Reynolds number case using the high Reynolds number DNS data ($Re_\theta = 2400$ [16]).

Figures 8 shows the scatter plots between the P term and λ_2 obtained for the decaying homogeneous isotropic turbulence. Overall, the result is similar to that for the channel flow, i.e., intense forward cascade is primarily associated with the sheet-like structure and the degree of an occurrence of the sheet-like structure is more enhanced compared with the mixing layer. However, it should be noted that the degree of an occurrence of the tube-like structure is not negligibly small compared with the channel flow.

3 Time development of the educed flow field in the channel flow

In this section, we pursue the time evolution of the educed flow field for the channel flow in Section 2. To do this, the effects of the SGS field must be correctly represented by the SGS models for the SGS stress tensor, τ_{ij}. We have used the dynamic two-parameter mixed model (DTM $C_B - C_S$ model [9]) obtained by linearly combining the SGS eddy viscosity coefficient model (the Smagorinsky model [17]) and scale-similarity model [18].

The assessment of the previous SGS models, Dynamic Smagorinsky model, [19] the dynamic mixed model, [20] the DTM proposed by Salvetti and Banerjee [21] and $C_B - C_S$ model, for wall-bounded and free shear flows [9] and the decaying compressible and

incompressible homogeneous isotropic turbulence have been previously reported. The $C_B - C_S$ model yielded the most accurate results in both "a priori" and "a posteriori" tests. Particularly important for the present study is the assessment results for the grid scale-SGS energy transfer. It was found in all of tested cases that the $C_B - C_S$ model is capable of accurate representation of both forward and backward scatters, while other models overestimate forward scatter and underestimate backward scatter. In fact, the $C_B - C_S$ model yielded a very accurate approximation for the distribution of the P_{11} term associated with the educed velocity field obtained in Section 2 (figure not shown).

Time evolution of the asymmetric streaky structure obtained for P_{11}-Forward event was pursued in LES using the $C_B - C_S$ model. The initial condition was given as the velocity and pressure fields derived from P_{11}−Forward case. With a lapse of time, the portion with positive contours catches up with that with negative ones, and the asymmetric streaky structure in Fig. 2 (a) was transformed into the symmetric streaky structure. Later, this symmetric structure became asymmetric again, in which the portion with positive contours were placed downstream of that with negative ones, similar to the contours shown in Fig. 2 (b) obtained for P_{11}-Backward event. Thereby, initially, an intense forward scatter occurred, and to relax this "excessive" generation of the SGS energy, the flow tended to adjust itself to reduce the cascade. It was found, however, that the turbulent state gradually decayed when the educed velocity field was directly used. This was because a lift-up of the low-speed streak was not strong enough to sustain the turbulence. [12)]

When the amplitude of turbulent fluctuations was set twice as large as those of the educed velocity field, a lift-up of the low-speed streak was initiated. Figure 9 shows the end view of time lines generated in the $x - z$ plane at $y_+ = 12$ for P_{11}-Forward case, after a non-dimensional time of $1.0tu_\tau/\delta$ elapsed. The time lines for the same plane and at the same instant obtained for P_{11}-Backward case are shown in Fig. 10. The degree of lift-up of low-speed streak shown in Fig. 9 is much larger than that shown in Fig. 10, implying that more intense lift up occurs in P_{11}-Forward event. It was found that this lift up was caused by a pair of counter-rotating streamwise vortices located above the detection point. It should be noted that this lift up did not occur uniformly along the low speed streak, but it was more manifested in the region where the high speed streak approaches the low speed streak. This result was consistent with that obtained in Fig. 10 that the region with the second largest lift up found in Fig. 10 ($z/\delta \simeq 1.0$) coincided with the region where the high speed streak approaches the low speed streak. It can be inferred that the largest lift up, or burst, is generated along P_{11}-Forward event, leading to the production of the small-scale (SGS) turbulent energy.

With the lapse of time, a lift up of the low-speed streak intensified and the low-speed streak located in the central region of the $x - z$ plane observed in Fig. 2 (a) was almost pumped out of the sublayer into the buffer layer. Thus, the wall vicinity became very tranquil. Figure 11 shows the contours of $\overline{u}''$ in the $x - z$ plane at $y_+ = 12$ obtained at $t = 2.2$. The low-speed streak in the central region of the $x - z$ plane is almost invisible, and the central region is mostly occupied with the high-speed fluid. Although another low-speed streak can be seen besides the central region, the amplitude of fluctuations along these streaks is not large enough to cause the lift up. In turn, the down wash (sweep) of the fluid in the region away from the wall into the near-wall region is initiated. Currently, we consider that this down wash was caused by a large scale streamwise vortices generated

by the Görtler type instability. With the injection of the high speed fluid, amplification and destabilization of the low-speed streak found in Fig. 11 occurs, as indicated in the contours of $\overline{u}''$ in the $x-z$ plane at $y_+ = 12$ obtained at $t = 3.8$ shown in Fig. 12, which leads to the lift up of these low-speed streaks.

We consider that a cyclical repetition of these three processes is the scenario in the sustenance of turbulence for the channel flow. More detailed investigation of these processes is currently underway.

Acknowledgment

This work was partially supported by the Grant-in-aid, Ministry of Education, Japan (No.10650162)

References

1) K. Horiuti, Phys. Fluids A1 (1989) 426.
2) U. Piomelli, T.A. Zang, C.G. Speziale and M.Y. Hussaini, Phys. Fluids A2 (1990) 257.
3) U. Piomelli, W.H. Cabot, P. Moin and S. Lee, Phys. Fluids A3 (1991) 1766.
4) C. Härtel, L. Kleiser, U. Friedemann and R. Friedrich, 'Phys. Fluids 6 (1994) 3130.
5) K. Horiuti, Phys. Fluids A 5 (1993) 146.
6) K. Horiuti, J. Phys. Soc. Japan 66, 91 (1997).
7) U. Piomelli, Y. Yunfang and R.J. Adrian, Phys. Fluids 8 (1996) 215.
8) P. Moin and J. Kim, J. Fluid Mech. 155 (1985) 441.
9) K. Horiuti, Phys. Fluids 9, 3443 (1997).
10) A.V. Johansson, P.H. Alfredsson and J. Kim, J. Fluid Mech. 224, 579 (1991).
11) J. Jeong, F. Hussain, W. Schoppa and J. Kim, J. Fluid Mech. 332, 185 (1997).
12) W. Schoppa and F. Hussain, Proc. IUTAM Symp. on Dynamics of Slender Vortices (ed. E. Krause), Aachen, Germany, 183 (1998).
13) W.T. Ashurst, A.R. Kerstein, R.M. Kerr and C.H. Gibson, Phys. Fluids 30, 2343 (1987).
14) A. Vincent and M. Meneguzzi, J. Fluid Mech. 225, 1 (1991).
15) M.M. Rogers and R.D. Moser, J. Fluid Mech. 243, 183 (1992).
16) M.M. Rogers and R.D. Moser, Phys. Fluids 6, 903 (1994).
17) J. Smagorinsky, Mon. Weath. Rev. 91, 99 (1963).
18) J. Bardina, Ph.D. dissertation, Stanford University, Stanford, California (1983).
19) M. Germano, U. Piomelli, P. Moin and W.H. Cabot, Phys. Fluids A 3, 1760 (1991).
20) Y. Zang, R.L. Street and J. Koseff, Phys. Fluids A 5, 3186 (1993).
21) M.V. Salvetti and S. Banerjee, Phys. Fluids 7, 2831 (1995).

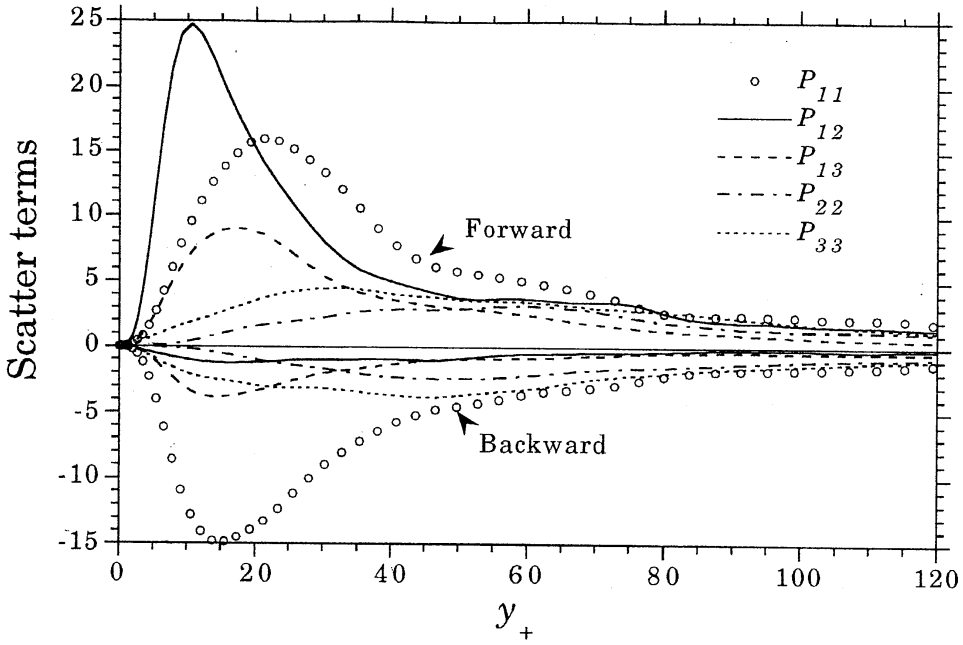

Figure 1 : y -distributions for plane-average of the individual terms in P, P_{ij}.

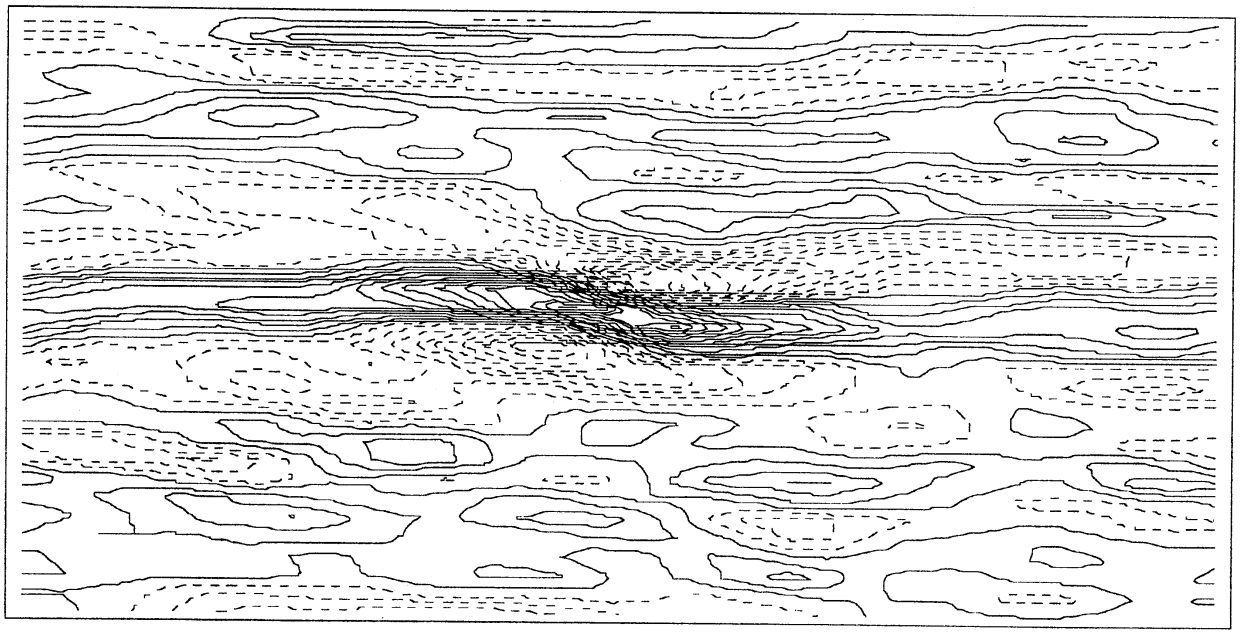

Figure 2 (a) : Top view of the contours for streamwise velocity in the x-z plane at $y_+ \sim 12$. (P_{11}-Forward event)

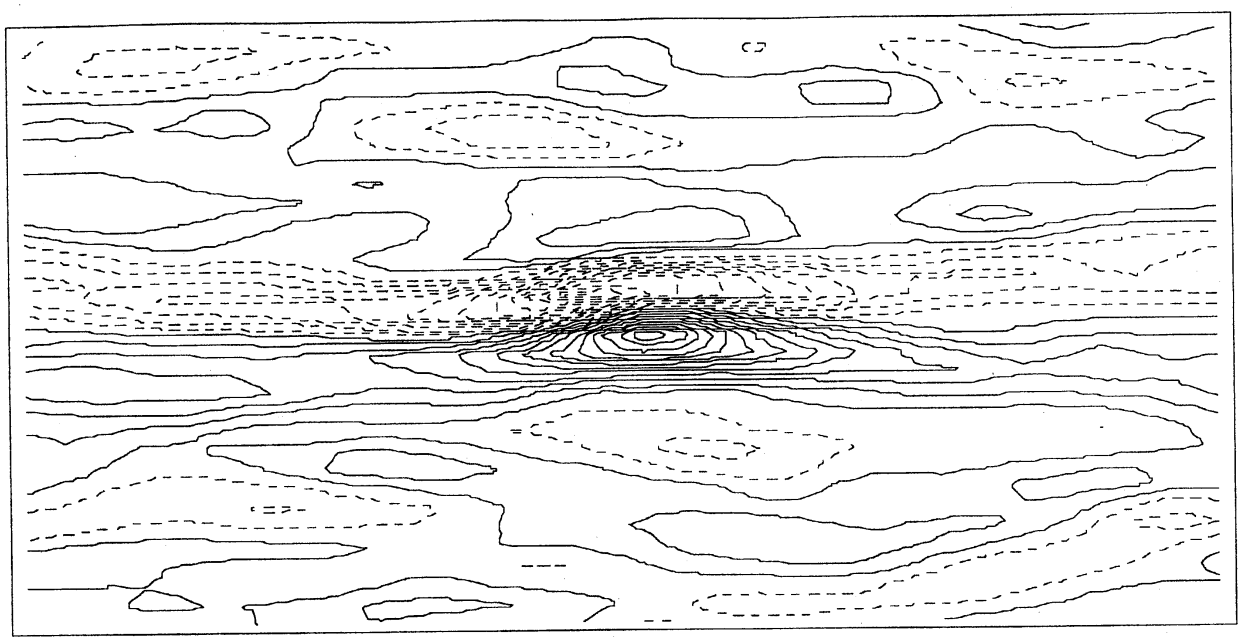

Figure 2 (b) : Top view of the contours for streamwise velocity in the x-z plane at y_+ ~ 12. (P_{11}-Backward event)

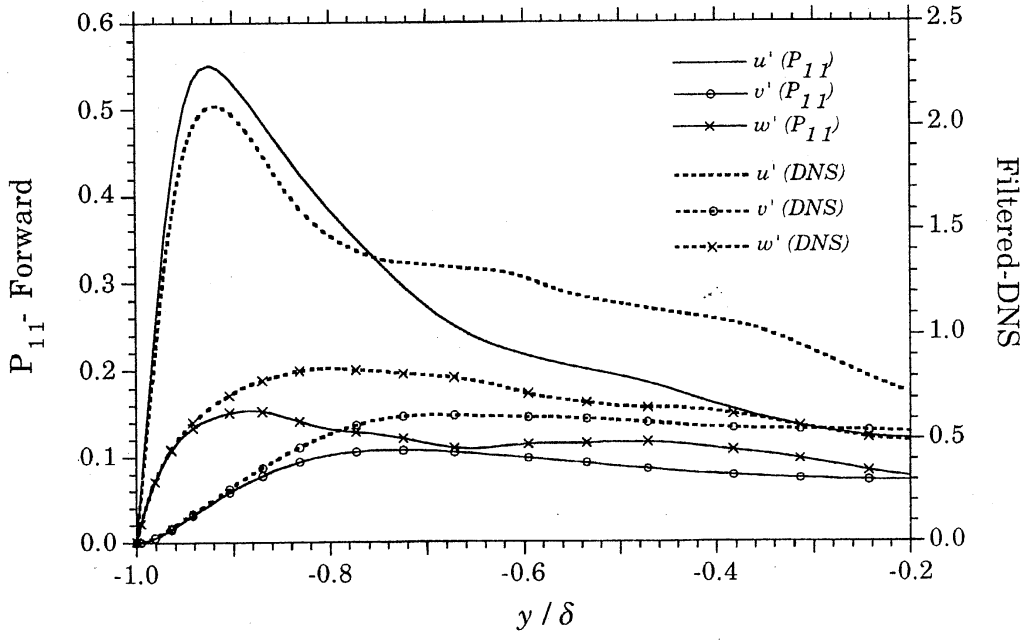

Figure 3 : y - profiles of the grid-scale turbulence intensities (P_{11}-Forward event).

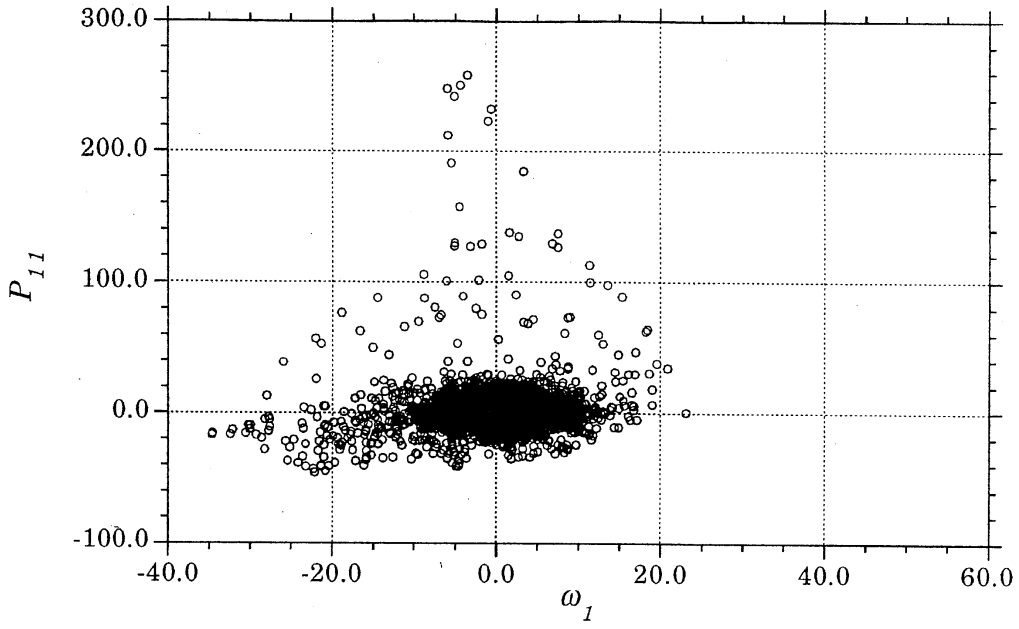

Figure 4 (a) : Scatter plots between the P_{11} term and the streamwise vorticity.

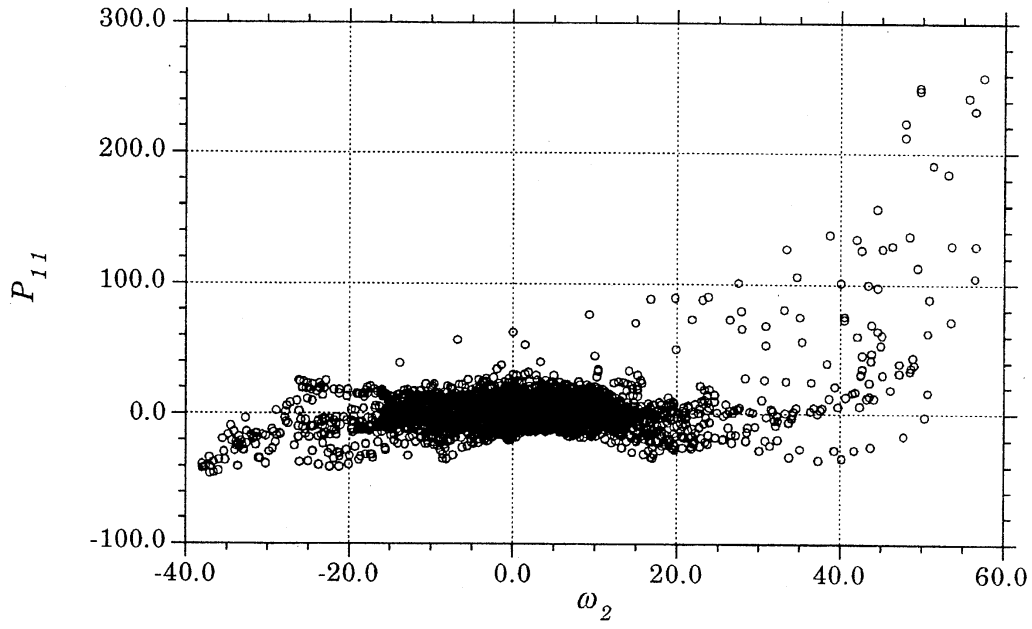

Figure 4 (b) : Scatter plots between the P_{11} term and the the wall-normal vorticity.

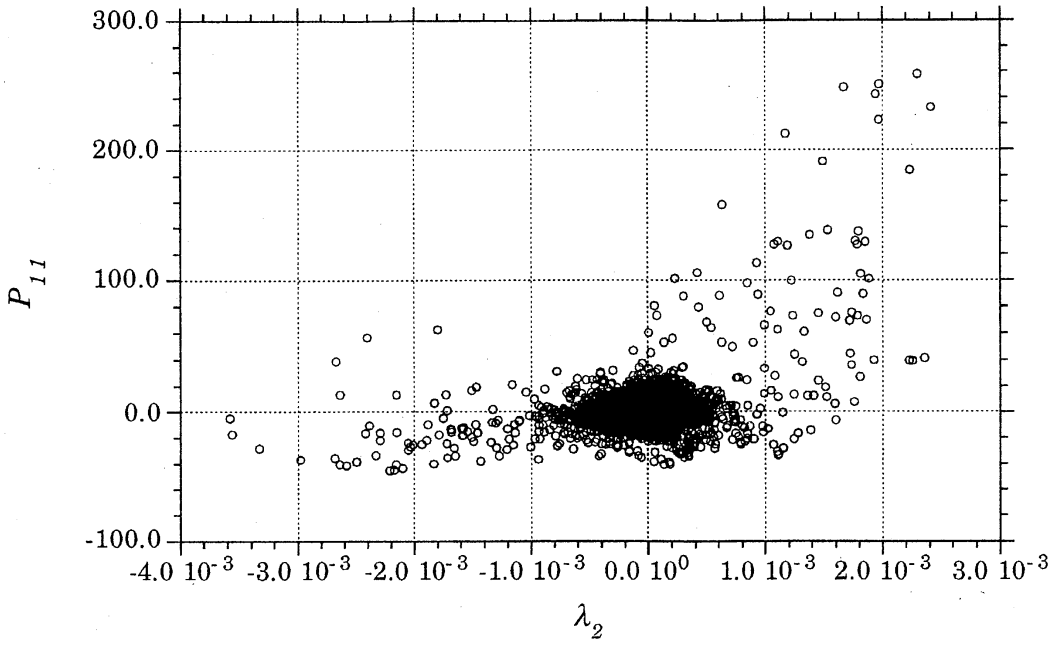

Figure 5 : Scatter plots between the P_{11} term and λ_2 for the channel flow.

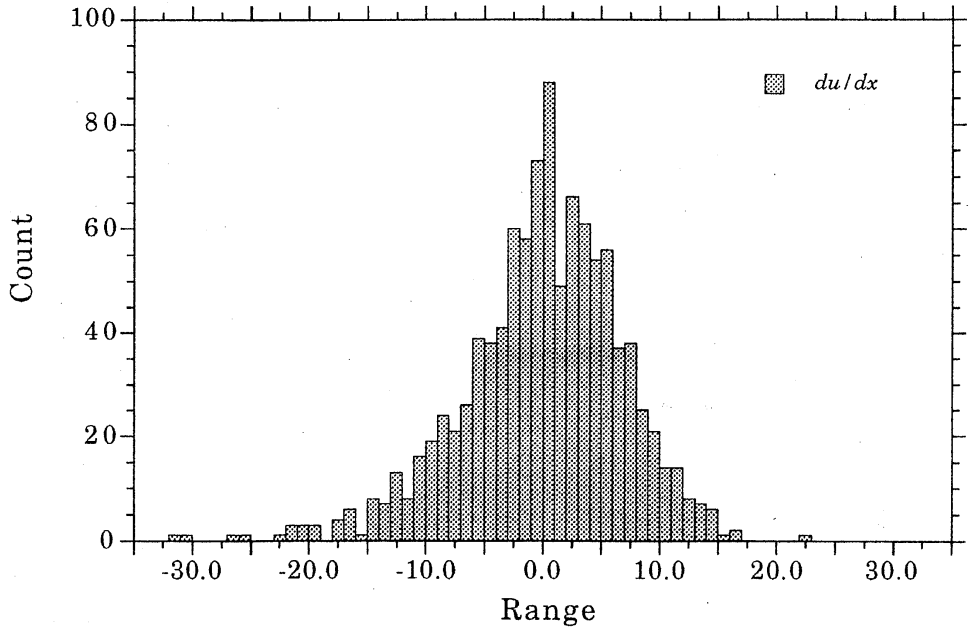

Figure 6 : Histogram for the longitudinal velocity derivative in the x-z plane at y_+=12, obtained from the filtered DNS data.

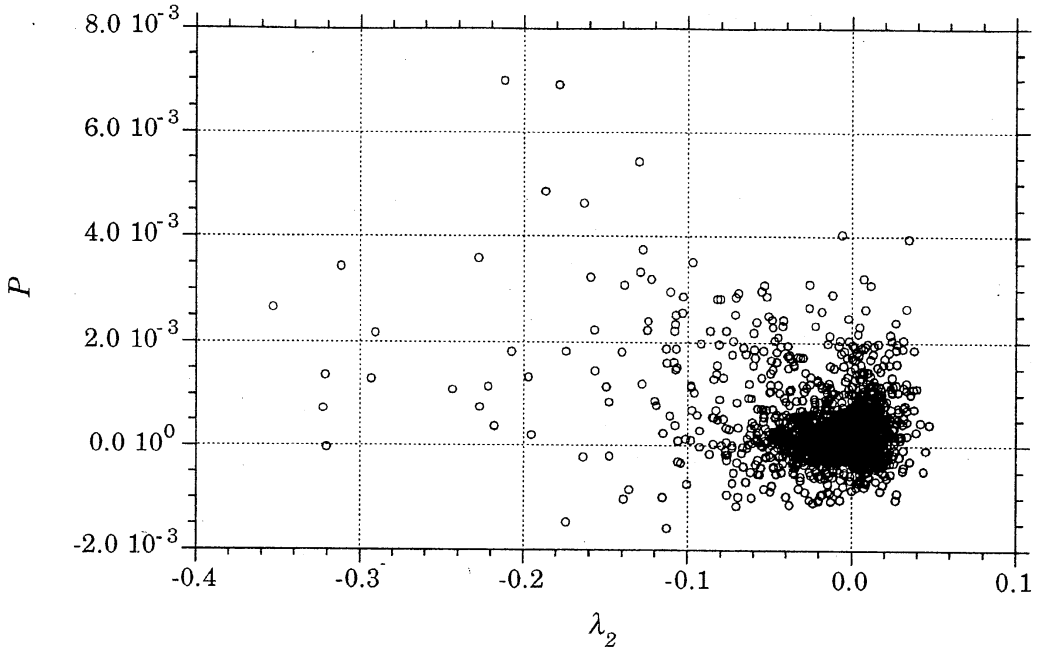

Figure 7 : Scatter plots between the P term and λ_2 for the mixing layer.

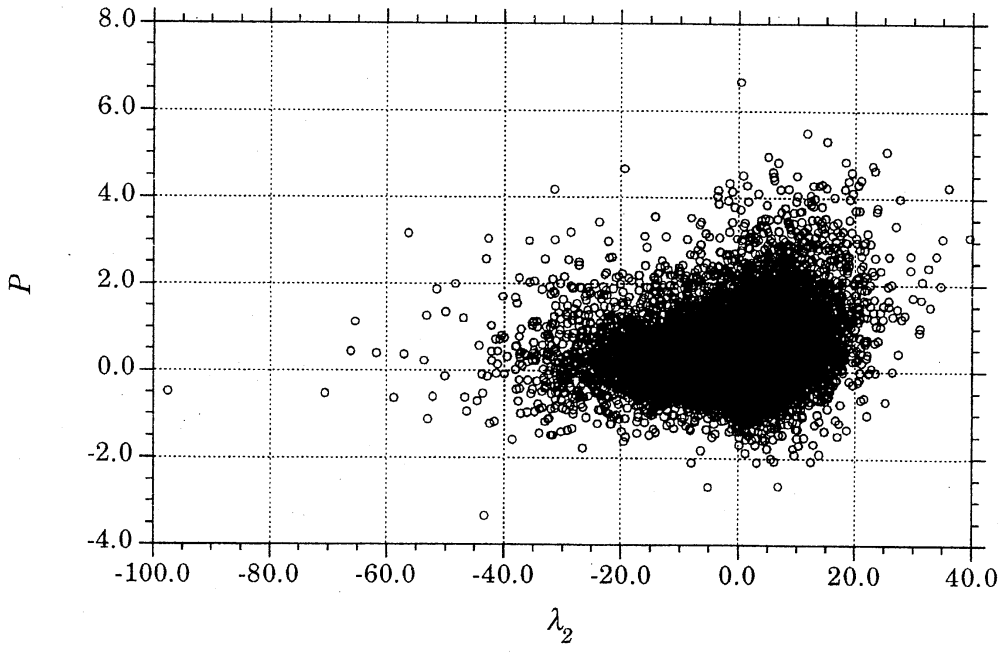

Figure 8 : Scatter plots between the P term and λ_2 for the decaying homogeneous isotropic turbulence.

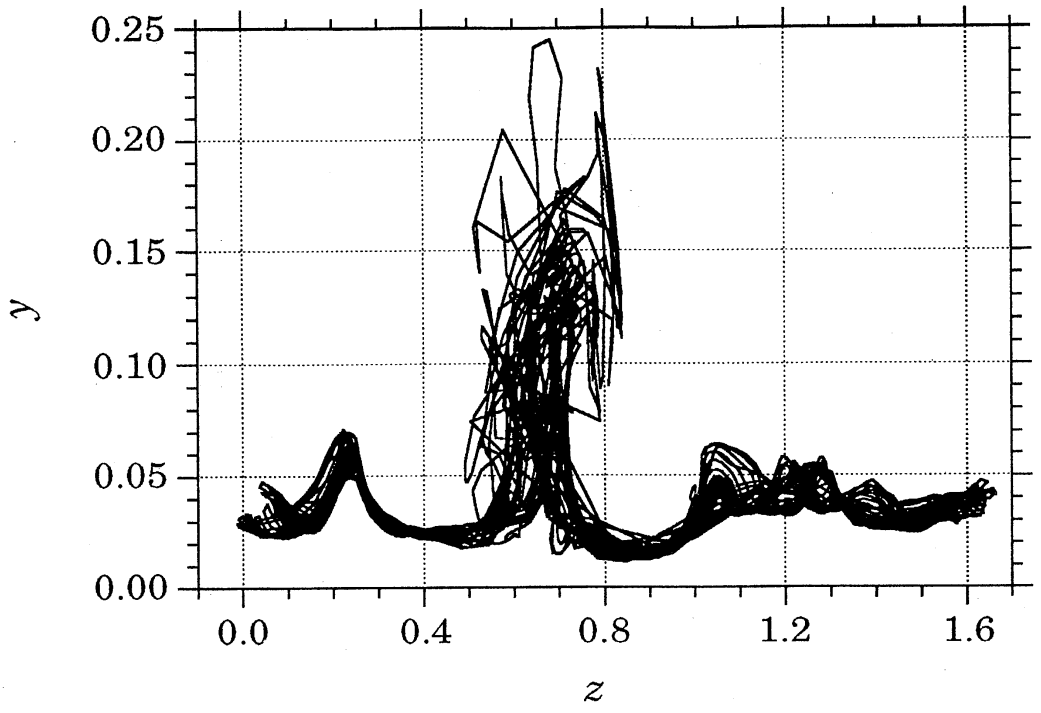

Figure 9: End view of time lines generated in the x-z plane at y+=12 from P_{11}-Forward case at $t\ \tau/\delta$ =1.0.

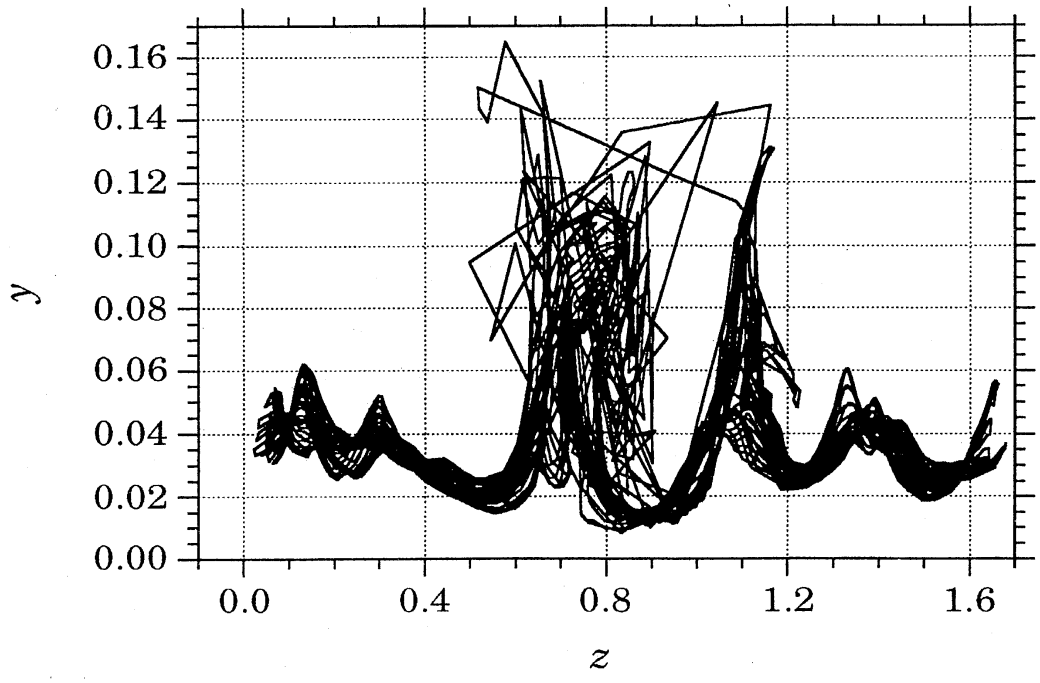

Figure 10 : End view of time lines generated in the x-z plane at y+=12 from P_{11}-Backward case at $t\ \tau/\delta$ =1.0.

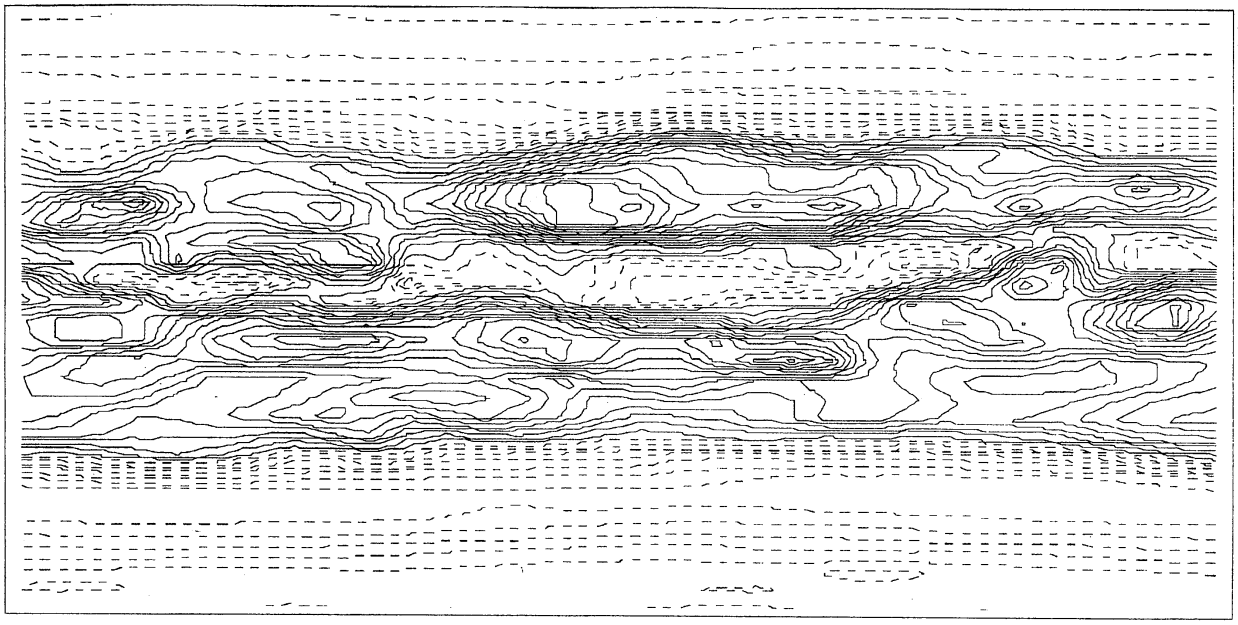

Figure 11 : Top view of the contours for streamwise velocity in the x-z plane at $y_+ \sim 12$ and $t = 2.2$

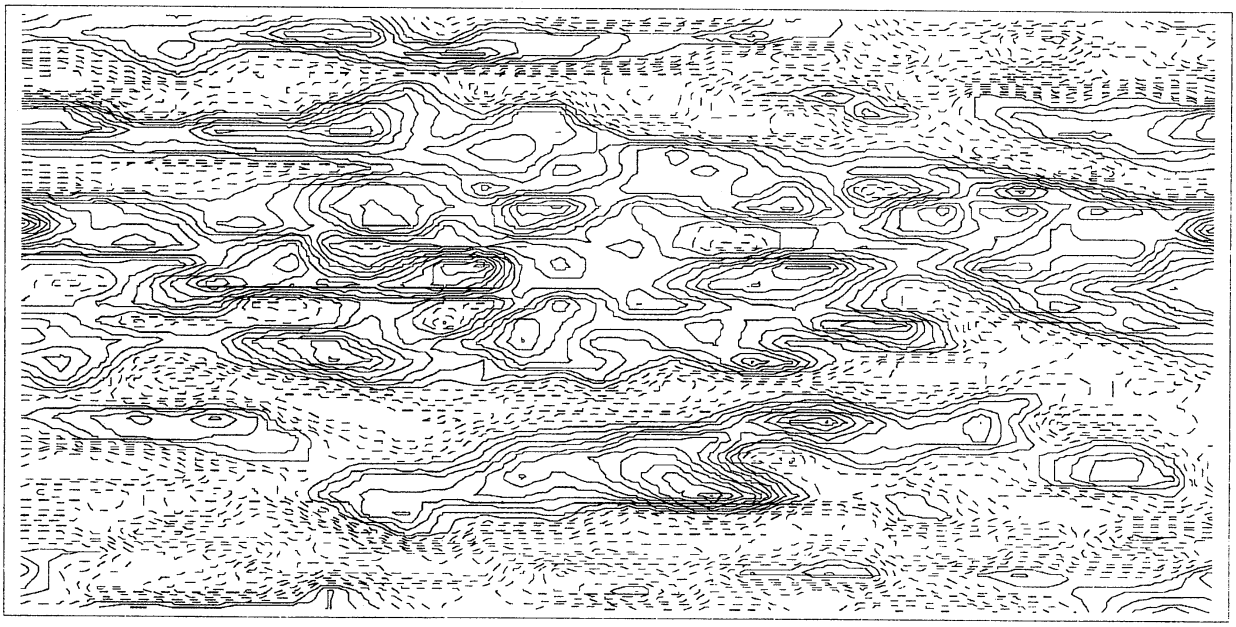

Figure 12 : Top view of the contours for streamwise velocity in the x-z plane at $y_+ \sim 12$ and $t = 3.8$